Separation Science and Technology
Publication details, including instructions for authors and subscription information:
http://www.informaworld.com/smpp/title~content=t713708471

A Study Toward the Scale-Up of Size-Exclusion Separations by Stagewise Countercurrent Contact

Partha Roy[a]; Johannes M. Nitsche[a]
[a] DEPARTMENT OF CHEMICAL ENGINEERING, STATE UNIVERSITY OF NEW YORK AT BUFFALO BUFFALO, NEW YORK, USA

To cite this Article Roy, Partha and Nitsche, Johannes M.(1997) 'A Study Toward the Scale-Up of Size-Exclusion Separations by Stagewise Countercurrent Contact', Separation Science and Technology, 32: 14, 2237 — 2266
To link to this Article: DOI: 10.1080/01496399708000767
URL: http://dx.doi.org/10.1080/01496399708000767

SEPARATION SCIENCE AND TECHNOLOGY, 32(14), pp. 2237–2266, 1997

A Study Toward the Scale-Up of Size-Exclusion Separations by Stagewise Countercurrent Contact

PARTHA ROY and JOHANNES M. NITSCHE
DEPARTMENT OF CHEMICAL ENGINEERING
STATE UNIVERSITY OF NEW YORK AT BUFFALO
BUFFALO, NEW YORK 14260, USA

ABSTRACT

This paper presents a theoretical and experimental exploration of the prospects for performing separations on size- or shape-polydispersed solutions of macromolecules or colloidal particles via multistage countercurrent contact between liquid and porous phases. Fractional extraction is shown to yield an arbitrarily sharp cut with sufficiently many stages. It is therefore possible in principle to sharpen a particle size distribution about any prescribed size (which can be varied by adjusting the liquid flow rate without changing the porous phase), and to achieve molecular shape-selective separations. Experiments are reported that demonstrate the relatively rapid attainment of partitioning equilibrium for colloidal polystyrene particles within a single-stage fixed-bed contactor packed with controlled-pore glass. A comprehensive convection-diffusion model explains a decaying temporal oscillation in the particle concentration arising in the experiments. Implications of the results for the large-scale processing of macromolecular and particulate dispersions are discussed. It is noted that the scale-up potential of the present technique is not restricted to separations by size-exclusion, and applies equally well in principle to affinity-based and other separations.

1. INTRODUCTION

The purpose of this paper is to explore theoretically and experimentally a separation system relying upon the partitioning of molecules or colloidal particles between a fluid phase and a porous solid phase by size exclusion (1). In practice, this and other microscopic partitioning phenomena are usually harnessed by two methods, both referred to by the name "chromatography": (i) true chromatography, which resolves a multicomponent mixture into separate traveling bands or peaks corresponding to the mo-

tion of solutes down a column or within an annulus at different speeds (2–4); and (ii) adsorption in a packed or fluidized column, which selectively removes one or more components (either the desired product or impurities) from the mixture (5, 6); cf. Ref. 7. The inherently multicomponent fractionation capability of (i) is ideal for analytical purposes, but carries with it the limitations of inherently batchwise operation [except in continuous annular systems (4)] and relatively small capacities in preparative applications (see Ref. 8, p. 460). Indeed, although the $O(100\text{L})$ packed volumes of some gel permeation columns fractionating $O(20–50)$ g of polymer or protein (3; 9, pp. 87–89) are certainly enormous by analytical standards, they represent capacities orders of magnitude smaller than typical unit operations, such as extraction (10), in chemical engineering. It is therefore not surprising that the largest-scale applications of gel permeation in pharmaceutical and foodstuff industries have often employed method (ii) (see Ref. 6, p. 203). Important examples include "desalting" (removal of low-molecular weight compounds) of whey and human serum albumin (5, 6). Here the column usually acts primarily to achieve a single cut between low- and high-molecular weight solutes, and thus performs one "group fractionation" as opposed to a full multicomponent resolution (6, 9).

There is some precedent for enhancement of the selectivity of this latter type of separation using multiple stages. Thus, for instance, Chang et al. (7) described protein extraction with a train of four mixer-settlers, although selectivity occurred here by affinity partitioning between two liquid phases. Also, continuous multistage countercurrent contact between fluid and solid phases is well developed within the context of adsorption processes, based either on actual motion of the solid phase or on simulated solids transport through cyclic motion of the fluid feed and product points (see, e.g., Refs. 11–13).

The specific objective of this paper is to investigate the possibility of achieving an arbitrarily sharp cut in a size- or shape-polydisperse solution of macromolecules or colloidal particles via multistage countercurrent contact between liquid and porous phases. Calculational methods from fractional extraction are applied in Section 2 to determine the required number of stages as a function of the desired sharpness of separation at a given molecular size, or between given molecular shapes. Experiments are reported in Section 3 on a single-stage contactor that achieves a relatively rapid partitioning equilibrium for spherical polystyrene particles within controlled-pore glass. Section 4 develops a model that explains the observed transient behavior, and yields an estimate of the particle Peclet number. Prospects for large-scale separations are discussed in Section 5.

2. SOLUTE SIZE- AND SHAPE-SELECTIVE EXTRACTION VIA PERMEATION

Since we apply classical concepts in extraction (10, 14), it is only necessary to outline very briefly the outcome of mass conservation and equilibrium relations as they apply here to a stagewise separation by permeation, depicted in Fig. 1. A feed stream with one (or more) dissolved solutes enters a cascade with oppositely directed flows of a solvent phase (volumetric flow rates S, $\bar{S}$) and a wetted porous phase (volumetric flow rates P, $\bar{P}$ representing total liquid plus solid volume). For the moment we shall observe the behavior of a *single* solute (drawing conclusions about multicomponent separations later) so there is no present need to distinguish different solutes (e.g., using a subscript i) in the dilute limit where one solute does not affect the permeation equilibrium of another. The phases enter pure (solute-free), and the desire is to predict and control the respective solute concentrations $\bar{x}^{[1]}$ and $y^{[1]}$ (moles or mass per volume) in the exiting $\bar{S}$ and P streams. Interphase contact occurs in stages, for which concentrations in the exiting streams satisfy a relation for permeation equilibrium, assumed for simplicity to have the form $y = Kx$. The flow rate of the solvent phase generally exhibits an abrupt increase (from S to $\bar{S} = S + F$) between sections immediately fore and aft of the stage where the feed is introduced, whereas $P = \bar{P}$. Small variations in flow rates caused by stage-to-stage changes in the solute concentrations are ignored, as is usual for dilute solutions.

Material balance and equilibrium relations for arbitrary stages m and n in the left and right sections, and for the feed stage, are expressible as

$$y^{[m+1]} = y^{[1]} + (S/P)x^{[m]}, \qquad y^{[m]} = Kx^{[m]} \tag{1}$$

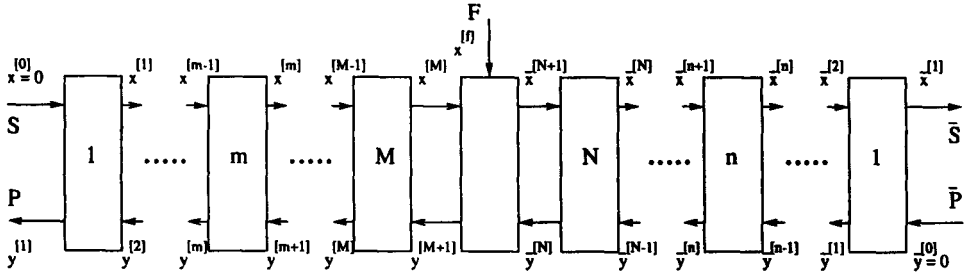

FIG. 1 Flow sheet for countercurrent contact between particle-bearing solvent and porous phases.

$$\bar{x}^{[n+1]} = \bar{x}^{[1]} + (\bar{P}/\bar{S})\bar{y}^{[n]}, \qquad \bar{x}^{[n]} = \bar{y}^{[n]}/K \tag{2}$$

and

$$Sx^{[M]} + Fx^{[f]} + \bar{P}\bar{y}^{[N]} = Py^{[M+1]} + \bar{S}\bar{x}^{[N+1]}, \qquad y^{[M+1]} = K\bar{x}^{[N+1]} \tag{3}$$

These equations can be combined to produce explicit formulas (representing variants of the "Kremser equation" (10, pp. 173–174, 235–237; 14, pp. 512–515) for the outlet concentrations, viz.,

$$y^{[1]} = Fx^{[f]}\,[(\bar{S}f_M - Sf_{M-1})/K + f_M(P - \bar{P}f_{N-1}/f_N)]^{-1} \tag{4}$$

$$\bar{x}^{[1]} = y^{[1]}f_M/f_N K \tag{5}$$

where for brevity $f_M \equiv f_M(S/PK)$, $f_N \equiv f_N(\bar{P}K/\bar{S})$, and $f_k(\alpha)$ denotes the function

$$f_k(\alpha) \equiv (1 - \alpha^{k+1})/(1 - \alpha) \tag{6}$$

[see Roy (18)]. The numerical values of $\bar{x}^{[1]}$ and $y^{[1]}$ depend critically upon the flow rates, the numbers of stages, and the partition coefficient K. In particular, the left-hand exiting solute concentration $y^{[1]}$ can be made arbitrarily small with sufficiently many stages if $K < S/P$, and $\bar{x}^{[1]}$ can similarly be made arbitrarily small if $K > \bar{S}/\bar{P}$.

Fractionation of a dilute multicomponent mixture occurs because species with $K < S/P$ exit predominantly on the right and species with $K > \bar{S}/\bar{P}$ exit predominantly on the left. In the interest of obtaining a sharp split, the ratios S/P and $\bar{S}/\bar{P}$ should be very close, i.e., the flow rate F of feed should be small relative to S. In practice, this requirement would be easy to meet by concentrating the incoming mixture so that only a little solvent is added to the countercurrent flow. Alternately, pure solvent could be extracted just before the feed stage by filtration to make $S = \bar{S}$. Thus, we shall usually regard S and $\bar{S}$ to be effectively identical.

2.1. Partition Coefficients for Porous Glass

Experiments reported below utilize a fixed bed packed with granules of glass that are themselves microporous, a common type of two-scale structure characterizable in terms of two distinct porosities. The symbol ϵ_{macro} is used here to denote the ratio of interstitial volume between the grains to the total packed volume (i.e., the interstitial or macroscopic porosity); ϵ_{micro} represents the microscopic porosity of the grains themselves. In terms of these quantities, the overall porosity ϵ (i.e., the fraction of the total volume occupied by fluid in a wetted packing) is given by

$$\epsilon = \epsilon_{macro} + (1 - \epsilon_{macro})\epsilon_{micro} \tag{7}$$

Our porous glass has $\epsilon_{macro} \cong 0.49$ and $\epsilon_{micro} \cong 0.69$ (see Section 3), which makes $\epsilon \cong 0.84$. As introduced above, the partition coefficient K gives the ratio of the superficial solute concentration [moles or mass of solute per total (liquid + solid) volume] in a porous phase to the bulk concentration in an adjacent fluid phase at equilibrium. It is given by the expression

$$K = \epsilon_{macro} + (1 - \epsilon_{macro})\epsilon_{micro}\langle\Phi\rangle(a) \tag{8}$$

which is very similar to Eq. (7). The crucial difference is the fact that K contains the single-pore partition coefficient $\Phi(a, R_p)$, representing the fraction of the total volume of a micropore of radius R_p accessible to the center of a solute of size a. It is this factor which imbues K with solute size and shape dependence, and thereby provides the basis for selectivity.

For a spherical solute of radius a within a circular cylindrical or spherical pore of radius R_p, Φ is given by

$$\Phi_{cyl\ pore}(a, R_p) = \begin{cases} (1 - a/R_p)^2, & a/R_p \leq 1 \\ 0, & a/R_p \geq 1 \end{cases} \tag{9}$$

$$\Phi_{sph\ pore}(a, R_p) = \begin{cases} (1 - a/R_p)^3, & a/R_p \leq 1 \\ 0, & a/R_p \geq 1 \end{cases} \tag{10}$$

(cf. Refs. 15, 16). For an infinitesimally thin rod of half-length a, Φ may be approximated to reasonable accuracy by the expressions

$$\Phi_{cyl\ pore}(a, R_p) = \begin{cases} 1 - (a/R_p) + (1/8)(a/R_p)^3 + (1/64)(a/R_p)^5, & a/R_p \leq 1 \\ (1/8)(a/R_p)^{-3} + (1/64)(a/R_p)^{-5}, & a/R_p \geq 1 \end{cases} \tag{11}$$

$$\Phi_{sph\ pore}(a, R_p) = \begin{cases} 1 - (3/2)(a/R_p) + (1/2)(a/R_p)^3, & a/R_p \leq 1 \\ 0, & a/R_p \geq 1 \end{cases} \tag{12}$$

derivable via straightforward considerations of analytic geometry (17, 18).

The angle brackets $\langle\ \rangle$ in Eq. (8) denote an average overall pore radii R_p. Our porous glass has such a narrow pore size distribution that negligible error is incurred in replacing $\langle\Phi\rangle(a)$ by $\Phi(a,R_p)$ based upon the nominal (mean) pore radius $R_p = 526.5$ Å (see Section 3 below). We estimate the single-pore partition coefficient to reasonable accuracy as the average

$$\Phi(a, R_p) = \alpha\Phi_{cyl\ pore}(a, R_p) + (1 - \alpha)\Phi_{sph\ pore}(a, R_p) \tag{13}$$

with equal weighting ($\alpha = 0.5$), although either pore model ($\alpha = 0$, $\alpha = 1$) would also be acceptable. Figure 2 shows the solute size dependence of the partition coefficient K predicted by Eqs. (8)–(13) for spherical and thin rodlike solutes. The sizes of both are characterized in terms of the mean projected radius r_m, which equals a for the sphere and $a/2$ for the rod.

2.2. Examples of Size- and Shape-Selective Separations

The operation of the basic fractional extraction scheme is quantified by Fig. 3(a), which shows the exiting solvent- and porous-phase concentrations ($\bar{x}^{[1]}$ and $y^{[1]}$, respectively) produced by a 21-stage extractor ($M = N = 10$) from a polydisperse feed having a uniform number distribution over particle diameters from 0 to 1000 Å. The notation $\bar{x}^{[1]}(a; S/P, \ldots)$, $y^{[1]}(a; S/P, \ldots)$ will be used to indicate explicitly the dependencies of $\bar{x}^{[1]}$ and $y^{[1]}$ upon the particle size a, as well as other operating parameters such as the ratio of flow rates S/P. In the present case $S/P = \bar{S}/\bar{P} = 0.5636$, which matches the value of the partition coefficient $K = 0.5636$

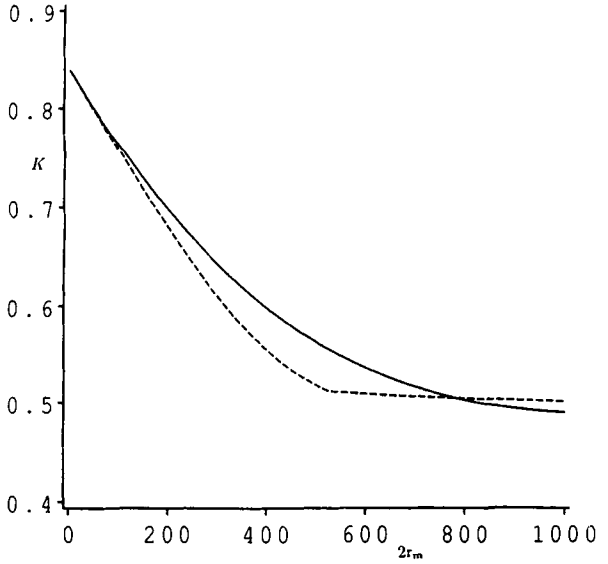

FIG. 2 Dependence of the partition coefficient K upon the mean projected radius (in Å) r_m for spherical (solid curve) and rodlike (dashed curve) solutes, based upon Eqs. (8)–(13) with $\alpha = 0.5$.

for 500 Å particles. The split therefore occurs at a diameter of 500 Å; particles smaller than this are concentrated in the (lower left) porous phase and particles larger than this are concentrated in the (upper right) solvent phase. Figure 3(b) shows the corresponding stream concentrations throughout the cascade. The maxima observed at the feed stage are a common feature of fractional extraction (10, pp. 232, 234).

A measure of the sharpness or selectivity of the split is provided by the maximum slope of the S-shaped curve giving $\bar{x}^{[1]}$ as a function of the particle diameter $2a$, i.e., the slope of this curve at its point of inflection. Moreover, the abscissa at the inflection point indicates the location of the split. Therefore, in all that follows we consistently use the equation

$$\frac{d^2(\bar{S}\bar{x}^{[1]}/Fx^{[f]})}{da^2}(a_0;\ S/P,\ \ldots) = 0 \tag{14}$$

to determine the value of S/P (or other parameters) needed to achieve a split at the prescribed particle size a_0. The selectivity of the split is then correspondingly defined as

$$\mathcal{S} \equiv \frac{1}{2}\frac{d(\bar{S}\bar{x}^{[1]}/Fx^{[f]})}{da}(a_0;\ S/P,\ \ldots) \tag{15}$$

In the case of Fig. 3, $\mathcal{S} = 1.52 \times 10^{-3}$ Å^{-1}. Figure 3(c) shows the increase in selectivity with increasing numbers of stages.

By performing two successive extractions it is possible to selectively strip a prescribed size fraction from a polydisperse suspension. The solid curves in Fig. 4 correspond to the situation where a first extractor ($S/P = \bar{S}/\bar{P} = 0.5802$) is used to strip particles smaller than 450 Å in diameter from the exiting solvent ($\bar{x}^{[1]}$) stream. This stream plays the role of feed for a second extractor ($S/P = \bar{S}/\bar{P} = 0.5490$) which then strips away particles larger than 550 Å from the exiting porous-phase ($y^{[1]}$) stream. The peak in $y^{[1]}$ centered at 500 Å becomes sharper as the number of stages increases. The dashed curves describe the corresponding outcome of two successive extractions with splits at 330 and 270 Å (flow rate ratios $S/P = \bar{S}/\bar{P} = 0.6587$ and $S/P = \bar{S}/\bar{P} = 0.6291$, respectively) designed to recover particles of diameter 300 ± 30 Å. These results suggest two interesting observations. First, within limits, the selected particle size can be changed simply by changing the ratio of flow rates S/P. It is unnecessary to alter the pore size of the packing. Second, a given packing operates best at a particle size corresponding to the mean of the extreme values of K. For the present porous phase, K ranges from 0.84 for effectively point-sized particles to 0.49 for 1053 Å (or larger) particles. Thus, it is most effective when it is used to strip particles with $K \cong 0.66$, which corresponds to a diameter of roughly 260 Å (dashed curves). Stripping of

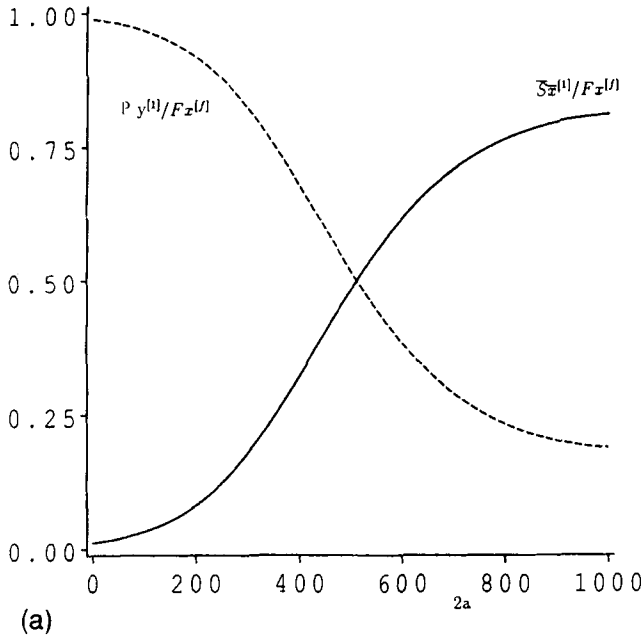

FIG. 3 Fractional extraction of a polydispersed mixture of spherical particles with $S/P = \bar{S}/\bar{P} = 0.5636$. (a) Solute fractions $\bar{S}\bar{x}^{[1]}/Fx^{[f]}$, $Py^{[1]}/Fx^{[f]}$ in the exiting streams as functions of spherical solute diameter $2a$ for operation with $M = N = 10$ stages. (b) Solute fractions $Sx^{[m]}/Fx^{[f]}$ and $\bar{S}\bar{x}^{[n]}/Fx^{[f]}$ in the solvent streams throughout the extractor for 500 Å (solid curve), 1000 Å (dot-dashed curve), and point-sized (dashed curve) solutes, for operation with $M = N = 10$ stages. (c) Selectivity $\mathcal{S}$ (ordinate) as a function of the number $M = N$ of stages.

500 Å particles (solid curves) is possible, although suboptimal in the sense that the peak shows a marked asymmetry (indicative of significant contamination of the product by large particles) if the number of stages is not sufficiently large.

Figure 5 addresses the separation of an equimolar mixture of spherical solutes with diameter $2a = 500$ Å and thin rodlike solutes with length $2a = 1000$ Å. These two solutes have equal mean projected radii (19) (i.e., equal "sizes"); selectivity therefore rests upon the shape difference. The ratio of the concentrations of spheres and rods in the exiting solvent phase is plotted as a function of the number of stages $M = N$ for $S/P = 0.5409$, which corresponds to the mean value of K for these two solutes (see Fig. 2 at abscissa $r_m = 500$ Å).

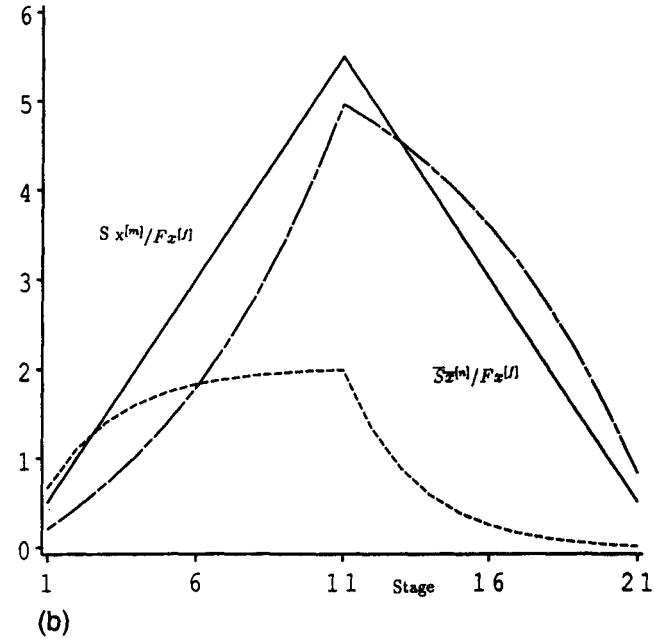

(b)

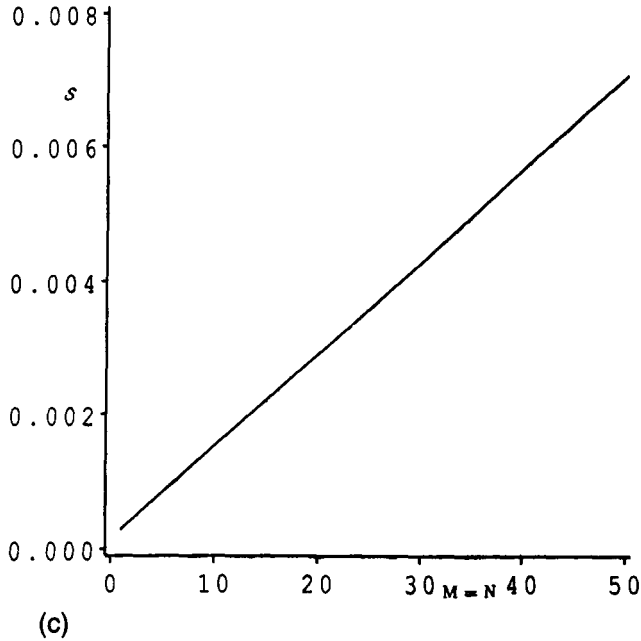

(c)

FIG. 3 Continued

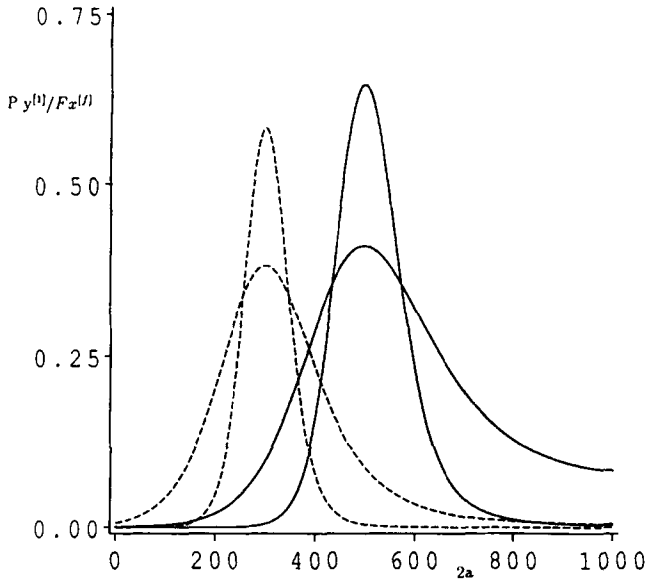

FIG. 4 Solute fraction $Py^{[1]}/Fx^{[f]}$ in the exiting porous phase from the second extractor as a function of solute diameter (in Å) for operation of two extractors in series. Solid curves: First extractor ($S/P = \overline{S}/\overline{P} = 0.5802$) produces a cut at 450 Å and second extractor ($S/P = \overline{S}/\overline{P} = 0.5490$) produces a cut at 550 Å. Dashed curves: First extractor ($S/P = \overline{S}/\overline{P} = 0.6587$) produces a cut at 270 Å and second extractor ($S/P = \overline{S}/\overline{P} = 0.6291$) produces a cut at 330 Å. Results are shown for $M = N = 20$ stages (broader peaks) and $M = N = 50$ stages (sharper peaks).

With the flow sheet of Fig. 1 the only way to enhance the selectivity $\mathcal{S}$ is to increase the number of stages (Fig. 3c). However, minor modifications of the scheme can, in principle, yield increases in $\mathcal{S}$ at a fixed number of stages, as is discussed in detail by Roy (18). One technique for achieving this end is suggested by the practice of liquid extraction, namely return of a fraction of each exiting flow to the cascade as reflux. Reflux ratios of order 100 are required to increase selectivity by a factor of 2 (18). This improvement comes at the expense of a much larger stage size (by a factor of the order of the reflux ratio) for given feed and product flow rates (needed to accommodate the larger volumes arising from recycle) and of higher particle concentrations throughout the cascade. An alternate approach for enhancing selectivity involves withdrawal of clear solvent at an intermediate stage. In the simplest case clear solvent is withdrawn only at the middle of the cascade (i.e., immediately to the left of the feed stage), which means that we allow S and $\overline{S}$ to differ. This approach en-

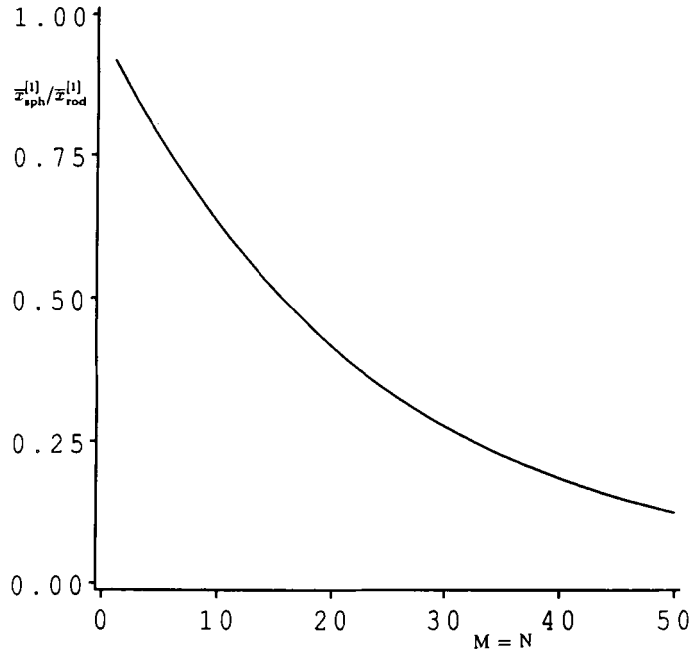

FIG. 5 Shape-selective separation carried out with $S/P = 0.5409$. The ratio of sphere to rod concentrations in the exiting solvent stream is plotted as a function of the number of stages $M = N$.

hances selectivity by making the xy operating line for the left section of the cascade steeper than that for the right section, in the parlance of liquid extraction, thereby widening the gap between the operating lines and the equilibrium curve ($y = Kx$). It has no literal counterpart in liquid extraction, where clear solvent cannot be removed from a chemical solution by filtration or centrifugation, as it can from a particulate dispersion. Withdrawal of clear solvent at an intermediate stage typically leads to enhancements in $\mathcal{S}$ by a factor of order 2 (18).

3. EXPERIMENTS WITH A SINGLE-STAGE CONTACTOR

Practical realization of the preceding developments hinges upon the ability to achieve a partitioning equilibrium between significant volumes of liquid and porous phases. It is essential to harness convection or mixing effects in order to transport solute particles to the surfaces of the porous

grains, because diffusion of colloidal particles over macroscopic distances is exceedingly slow. Although a mixer-settler would seem a priori to be a good contactor, we encountered difficulties in the respect that agitation produced unwanted fines by mechanical breakage of the porous solid. We therefore resorted to a contacting scheme based upon flow through a fixed bed. This section documents our preliminary experiments aimed at characterizing the operation of this equipment, regarded as a single stage of a cascade.

3.1. Materials and Instrumentation

Controlled pore glass was obtained from CPG, Inc. (Lincoln Park, NJ) for use as the porous phase. This material (product number CPG01000C, lot number 08C025) had the form of a white powder comprising roughly 35–70 μm grains possessing an essentially monodisperse distribution of micropores with diameter 1053 Å ± 4.3%. It was used in "as is" condition as supplied by the manufacturer. Electron micrographs roughly confirmed the stated micropore diameter and grain size. Porosity values were estimated by soaking 30 g of dry glass overnight with excess water, decanting off the supernatant water, and then reweighing to determine the amount of absorbed water. This total water content comprised interstitial and microporous contributions, the latter given as 1.06 cm^3/g of dry glass by CPG, Inc. The dry glass volume was estimated assuming a pure glass density equal to that of silica, i.e., 2.2 g/cm^3 (cf. Ref. 20). This mass-based procedure yielded the values $\epsilon_{macro} = 0.49$ and $(1 - \epsilon_{macro})\epsilon_{micro} = 0.35$, and indicated a total (liquid + solid) volume consistent to within $O(1\%)$ of a direct measurement of the total volume.

Polystyrene latex microspheres of three different sizes (diameters roughly 160, 520, and 1000 Å) were obtained from Bang's Laboratories, Inc. (Carmel, IN) to serve as model colloidal solutes. The particles were supplied in the form of aqueous suspensions stabilized with an anionic mixed sulfonate surfactant (520 Å) or an anionic fatty acid surfactant (160, 1000 Å) at concentrations below the critical micelle concentration (CMC). For 160 and 1000 Å particles, some sodium dodecyl sulfate (SDS) was added (below the CMC) to stabilize the solutions and prevent any particle agglomeration, in response to anomalies in the measured partition coefficients (see below). The particle suspensions were diluted down to concentrations lying in the dilute concentration range ($\leq 0.1\%$ by weight) (21).

Purified water from a Millipore Milli-Q UF Plus system was used for all solutions and experiments.

A Hach model 2100N turbidimeter was used to measure particle concentrations. The optical reading I in nephelometric turbidity units ("n.t.u.")

was calibrated against particle concentration (x or y in mg/mL). Calibration curves obtained from known dilutions in the 0.125–1.0 mg/mL range were linear. Measured concentrations in the experiments reported below yielded turbidities lying well within the operative range of the instrument (0 to 4000 n.t.u.), for which the accuracy of measurements is ±2% of the reading and repeatability is ±1% according to the manufacturer.

Further details on materials and instrumentation are given by Roy (18).

3.2. Single-Stage Contactor

Fixed beds were constructed in a Buchner funnel fitted with a perforated ceramic plate and a 1.0-μm pore size filter paper, and placed on top of a 750-mL glass column with a stopcock and a hose leading to a pressure gauge and aspirator pump (Fig. 6). The funnel was filled with water, and a known weight of dry glass was poured gently into the slowly draining pool to form a wetted packed bed after draining off the excess water.

Packed beds of two sizes were used, respectively identified as "small" or "large." The small bed was made with a 5.5-cm diameter funnel, contained approximately 30 g of dry glass, and had a packed height of about 3.2 cm. A pressure drop of roughly 10 in.H_2O was needed to maintain a liquid flow rate through it of $\dot{Q}_S$ = 8–10 mL/min. The large bed was made

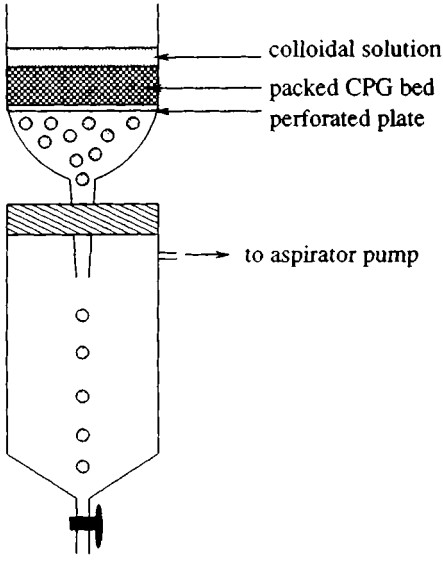

FIG. 6 Schematic diagram of the experimental apparatus.

with a 9-cm diameter funnel, contained approximately 90 g of dry glass, and had a packed height of about 4.5 cm. The required pressure drop for a flow rate of $\dot{Q}_S$ = 30 mL/min was roughly 8 in.H_2O. The preceding pressure drops are consistent with the Leva correlation (22, p. 5-53). Before use, the beds were washed repeatedly until most of the glass fines were removed and the turbidity of the exiting washwater dropped below 0.2 n.t.u.

The experiments conducted are typified by the following steps (in terms of amounts appropriate to the small bed): (i) preparation of approximately 40 mL of fresh colloidal suspension and measurement of its turbidity; (ii) addition of half this suspension (i.e., 20 mL) to the top of the bed, followed by vacuum-driven flow for one-half cycle time ($T_{flow}/2$) until the liquid level dropped to the surface of the glass packing; (iii) release of the liquid (20 mL) collected in the glass column, combination with the remaining 20 mL of fresh suspension, and measurement of its turbidity over a time period $T_{no\ flow}$; (iv) addition of the resulting 40 mL of liquid to the top of the bed, followed by vacuum-driven flow for one full cycle time (T_{flow}) until the liquid level dropped to the surface of the glass packing; (v) release of the liquid (40 mL) collected in the glass column, and measurement of its turbidity over a time period $T_{no\ flow}$. Steps (iv) and (v) were repeated until two successive turbidity readings were within 2% of each other. The purpose of dividing the initial charge of liquid, and of recycling the liquid, was to enhance mixing and reduce the time needed to reach partitioning equilibrium, as is discussed further in Section 4. Cycle times T_{flow} of both 3 and 5 minutes were tried; no significant difference in the value of K accompanied the change in cycle time. The results represented in Fig. 10 below refer to experiments with 520 Å particles carried out in the small bed (with T_{flow} = 3 and 5 min) and the large bed (with T_{flow} = 3 min). Experiments with 160 Å particles were carried out in the large bed (with T_{flow} = 5 min) and experiments with 1000 Å particles were carried out in the small bed (with T_{flow} = 5 min). Details are given by Roy (18).

3.3. Results

Figures 7 and 8 show typical results for the measured turbidity during the approach to partitioning equilibrium, and during regeneration of the small bed, for 520 Å particles. It is seen that equilibrium is effectively reached after approximately 6–7 cycles. The oscillatory nature of the curve in Fig. 7 arises from a mixing phenomenon explained in Section 4. A comparison was made of the mass of particles in the original suspension and the mass of particles in the solvent and porous phases after partitioning had been allowed to occur. All masses were computed from turbidimet-

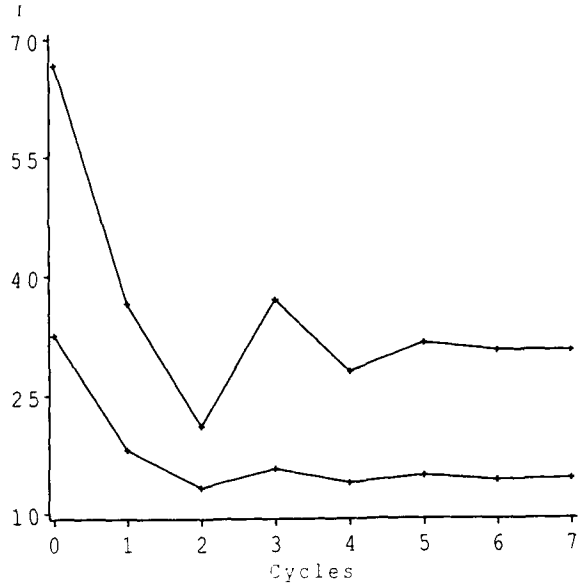

FIG. 7 Volume-averaged turbidity (I) of the exiting solution as a function of the number of cycles (passes through the bed) for 520 Å particles in the small bed.

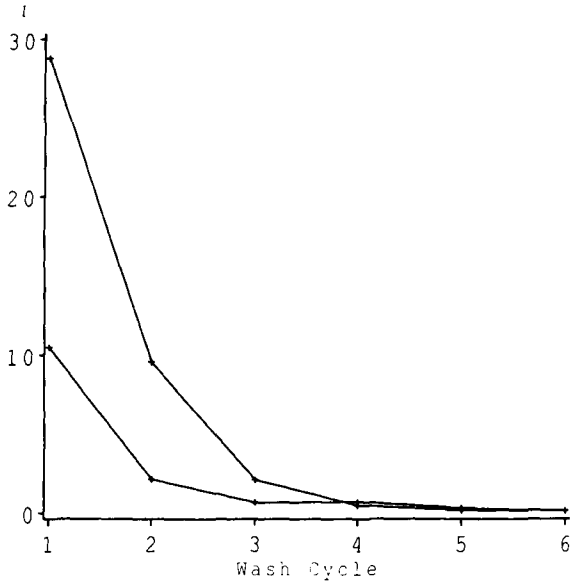

FIG. 8 Bed regeneration by washing. Volume-averaged turbidity as a function of the number of washes for 520 Å particles in the small bed.

ric measurements, and the particle content of the porous phase was determined during bed regeneration by washing. The particle material balance was found to be satisfied to within 5%. Figure 9 is the counterpart of Fig. 7 for the large bed, and shows that the operation proceeds in essentially the same way at three times the volume.

Initially, the measured turbidities for the 160 Å particles rose slowly with increasing number of cycles following the initial rapid drop and oscillations, and therefore did not appear to settle down to an equilibrium value. Conversely, the measured turbidities for the 1000 Å particles dropped slowly [see Roy (18)]. Both these undesired phenomena were eliminated by adding sodium dodecyl sulfate (SDS) (below the CMC of 2.5 mg/mL, at concentrations ranging from 0.5 to 1.5 mg/mL), and all data reported here for 160 and 1000 Å particle sizes refer to suspensions treated with SDS. All the 160 Å particles absorbed by the bed could be accounted for to within roughly 5% in the washwater. The 1000 Å particles seemed to elute from the bed slowly, judging from the fact that the washwater showed significant turbidity even after 8–10 washes. Curiously, however, the turbidimetrically determined particle content of the bed was appar-

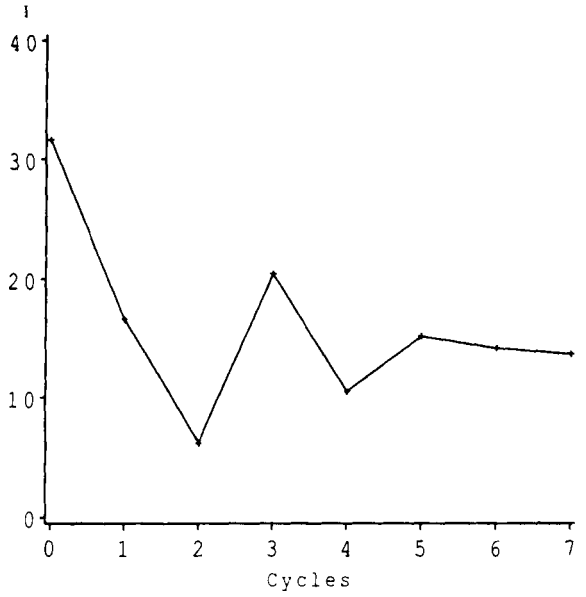

FIG. 9 Volume-averaged turbidity of the exiting solution as a function of the number of cycles for 520 Å particles in the large bed.

ently too large, violating mass conservation by as much as 40% in one experiment. These anomalous phenomena observed during washing of 1000 Å particles from the bed remain to be resolved and are discussed by Roy (18). It is worth noting, however, that partition coefficients determined for these particles (see below) are nevertheless roughly consistent with theoretical expectations.

Values of the partition coefficient K were calculated from the equation

$$K = \frac{I_0 V_0 - I_f V_f}{V_p I_f} \tag{16}$$

where V_0 and I_0 denote the volume and turbidity of the initial (fresh) suspension, V_f denotes the final volume of collected solution, I_f denotes the average of the last two turbidity readings, and V_p denotes the porous phase volume. The volume V_f of solution collected at the end of a run was somewhat smaller than the initial volume V_0 due to losses in liquid transfers, but only by about 1–2%.

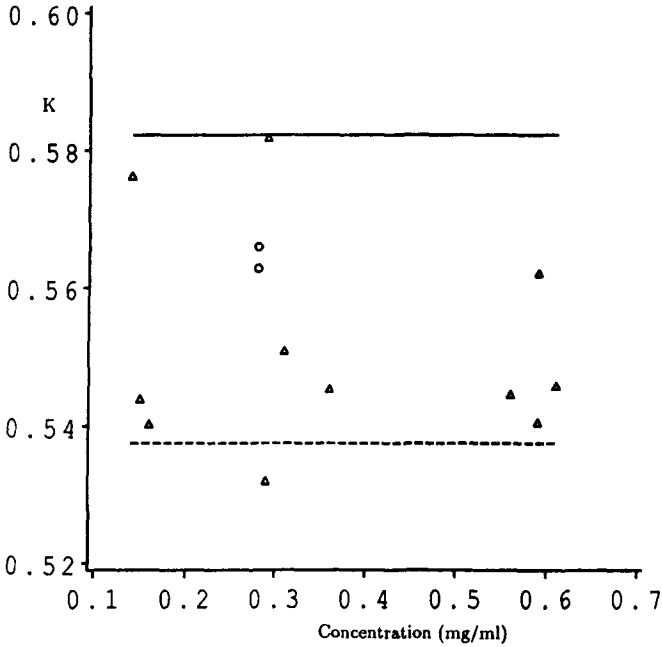

FIG. 10 Partition coefficient K versus concentration (mg/mL) for 520 Å particles. The experimental data are represented by triangles for the small bed and circles for the large bed. Horizontal lines correspond to theoretical predictions for cylindrical (solid line) and spherical (dashed line) pore models.

Figure 10 shows 13 individual determinations of K for the 520 Å particles at various dilute concentrations (obtained from the calibration of turbidity against concentration) in the two packed beds, and gives an indication of the degree of scatter observed. Data at concentrations of roughly 1 mg/mL or higher showed more scatter, and are not given here [see Roy (18)]. Five determinations of K for the 160 Å particles in the large bed and four determinations of K for the 1000 Å particles in the small bed showed greater scatter than that evident in Fig. 10. The large bed was used to determine K for the 160 Å particles due to better flow control in the bed and less glass fines. The presence of small amounts of glass fines can significantly affect the turbidity readings in the range of 0–2 n.t.u., at which the 160 Å particles are detected, and thus contributed to the larger scatter observed in the K values. Figure 11 compares the average values of K determined for each of the three particle sizes with the theoretical predictions of circular cylindrical and spherical pore models (cf. Eq. 13

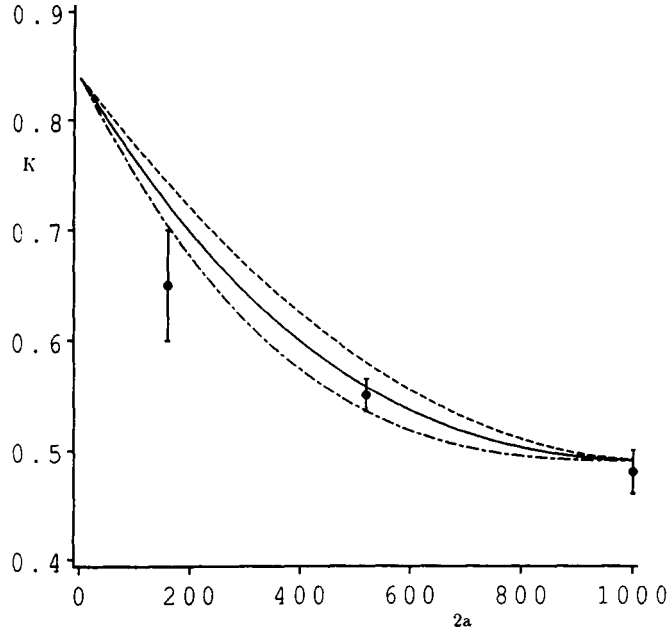

FIG. 11 Average values of the partition coefficient K determined experimentally for the 160, 520, and 1000 Å particles (indicated with circles). Theoretical curves represent Eq. (13) with $\alpha = 1$ (dashed curve, cylindrical pore model), $\alpha = 0$ (dot-dashed curve, spherical pore model), and $\alpha = 0.5$ (solid curve, equal weighting of the two pore models).

with $\alpha = 1$ and $\alpha = 0$, respectively). Both models seem to represent the results to within experimental uncertainty, which is greatest for the 160 Å particles. We regard Eq. (13) with equal weighting of the cylindrical- and spherical-pore inputs ($\alpha = 0.5$) as a reasonable descriptor of the partitioning data.

We conclude that it is feasible to achieve a partitioning equilibrium between significant volumes of a particle-laden fluid phase and a porous solid phase within a few contacting cycles.

4. A MODEL OF THE SINGLE-STAGE CONTACTOR

The recycle flow used in the experiments to achieve contact between solvent and porous phases gave rise to an oscillatory dependence of the particle concentration in the eluted liquid upon the number of cycles. The basic underlying mechanism for this behavior can be understood with reference to the simple hypothetical case of zero dispersion and impermeable grains. The initial charge of particle-laden suspension (concentration C_{bulk}) simply displaces clear (particle-free) solvent from the bed. Thereafter, recycle of this clear eluant to the top of the bed leads to a displacement of the particle-laden suspension. Thus, if the recycle volume equals the interstitial volume, then the concentrations of succeeding batches of eluted liquid must alternate interminably between 0 and C_{bulk}. The purpose of adding only half of the initial charge of particle-laden suspension to the bed, and of mixing the remaining half with the eluted liquid, in the first cycle is to help break up this displacement process by providing an opportunity for mixing to occur outside the bed. It is shown elsewhere (18) that the measured eluent concentrations are bracketed by curves representing the limiting cases of zero dispersion and perfect mixing. This fact serves as an overall check on the experimental procedure, and indicates that a quantitative model must account for a finite degree of dispersion. We now develop such a model.

Each cycle comprises a period of duration $T_{flow}/2$ or T_{flow} during which a volume of liquid V_S undergoes gravity- and pressure-driven flow through the bed, and a subsequent period of duration $T_{no\ flow}$ during which the bed sits idle (while the turbidity of the collected drained liquid is being measured). In both periods, particles undergo transport between the interstitial voids and the porous grains (taken to be spherical). The particle contents of these two phases are quantified in terms of the respective concentrations C_i and C_p (solute per liquid volume), both of which vary with time T and axial position Z. The intragrain concentration field C_p depends, in addition, upon the microscopic radial coordinate R.

Flow Conditions. During flow through the bed, the two concentration fields are governed by the equations [see, e.g., Yau et al. (23); cf. Yang (24, pp. 101–104)]

$$\frac{\partial c_i}{\partial t} + \frac{\partial c_i}{\partial z} - \frac{1}{\mathrm{Pe}}\frac{\partial^2 c_i}{\partial z^2} = -q(z, t), \qquad 0 < z < 1, \quad t > 0 \tag{17}$$

$$\frac{\partial c_p}{\partial t} = \beta\left(\frac{\partial^2 c_p}{\partial r^2} + \frac{2}{r}\frac{\partial c_p}{\partial r}\right), \qquad 0 < r < 1, 0 < z < 1, \quad t > 0 \tag{18}$$

cast in terms of the dimensionless quantities

$$t = TV/L;\ z = Z/L;\ r = R/A;\ c_i = C_i/C_{\mathrm{bulk}};\ c_p = C_p/C_{\mathrm{bulk}};\ \mathrm{Pe} = VL/D_i \tag{19}$$

where L denotes the length of the bed, A is the radius of the grains, V is the mean fluid flow velocity through the bed, D_i is the dispersion coefficient, and C_{bulk} is the concentration of the starting colloidal suspension. The dimensionless group Pe has the significance of a Peclet number for mass transfer. The group β is given by

$$\beta = LD_p/A^2V \tag{20}$$

with D_p the effective diffusivity of the particles within the grains. The symbol q, discussed below, represents the volumetric rate of particle flow into the porous grains.

The initial distributions

$$c_i(z, 0) = f_i(z); \qquad c_p(r, z, 0) = f_p(r, z) \tag{21}$$

defined over the interval $0 < z < 1$ are either identically zero (at the beginning of the very first cycle) or else determined by the evolution of the previous cycle. The boundary conditions imposed upon the interstitial and porous-phase concentrations for all times $t > 0$ are

$$c_i(0, t) - \frac{1}{\mathrm{Pe}}\frac{\partial c_i}{\partial z}(0, t) = 1 \tag{22}$$

$$\frac{\partial c_i}{\partial z}(1, t) = 0 \tag{23}$$

$$\frac{\partial c_p}{\partial r}(1, z, t) = \kappa[c_i(z, t) - c_p(1, z, t)] \tag{24}$$

$$c_p \text{ finite at } r = 0 \tag{25}$$

Use of the "Danckwerts boundary conditions" (25) (Eqs. 22 and 23) is discussed, e.g., by Brenner (26) and Novy et al. (25), and we adopt them

here as a simple description of mass transfer processes occurring at the ends of the bed. Equation (24) couples the interstitial and porous-phase concentrations by equating, at each locale z, the flux of particles from the grain surfaces to their interiors and from the bulk interstitial fluid to the grain surfaces. The latter is expressed in terms of a mass transfer coefficient k, and

$$\kappa = kA/D_p\epsilon_{micro}\Phi \tag{26}$$

represents a dimensionless version of this coefficient. The volumetric rate q appearing in Eq. (17) is proportional to this common flux, viz.,

$$q = \frac{3(1 - \epsilon_{macro})}{\epsilon_{macro}} \epsilon_{micro}\Phi\beta \frac{\partial c_p}{\partial r}(1, z, t)$$

$$= \frac{3(1 - \epsilon_{macro})}{\epsilon_{macro}} \epsilon_{micro}\Phi\beta\kappa[c_i(z, t) - c_p(1, z, t)] \tag{27}$$

The dimensional concentration of the accumulated eluent from the bed is given by the average

$$\overline{C} = (C_{bulk}/t_{flow}) \int_0^{t_{flow}} c_i(1, t)\, dt \tag{28}$$

No-Flow Conditions. In the absence of flow, molecular diffusion produces negligible z-directed transport over macroscopic distances. Thus, the interstitial concentration changes solely by local molecular diffusion of particles into or out of the porous grains. This state of affairs is described by the differential equations

$$\frac{\partial c_i}{\partial t} = -q(z, t), \qquad 0 < z < 1, \quad t > 0 \tag{29}$$

$$\frac{\partial c_p}{\partial t} = \beta\left(\frac{\partial^2 c_p}{\partial r^2} + \frac{2}{r}\frac{\partial c_p}{\partial r}\right), \qquad 0 < r < 1, 0 < z < 1, \quad t > 0 \tag{30}$$

The dimensionless time t and the group β are here redefined as $t = TD_\infty/A^2$ and $\beta = D_p/D_\infty$, with D_∞ the bulk particle diffusivity, because a convective time scale ceases to exist in the absence of flow. All other dimensionless variables are as given by Eq. (19). The initial distributions in Eq. (21) now derive from c_i and c_p at the end of the immediately preceding flow period. Boundary conditions are not imposed upon c_i because Eq. (29) is an ordinary differential equation in which z enters only as a parameter. Equations (24) and (25) still apply.

Impermeable Grains. If the particles are too large to permeate into the porous grains, then q is identically zero, and all transport equations pertaining to the porous phase are ignored. This means, in particular, that the interstitial concentration undergoes no changes during the no-flow period.

The Washing Process. The process by which the bed starts out saturated with solute and is washed with clear solvent is described by the preceding equations with the modifications that Eqs. (21) and (22) are replaced with the following initial and boundary conditions:

$$c_i(z, 0) = 1, \; c_p(z, 0) = 1, \qquad 0 < z < 1 \tag{31}$$

$$c_i(0, t) - \frac{1}{\mathrm{Pe}} \frac{\partial c_i}{\partial z}(0, t) = 0 \tag{32}$$

Here c_i is made dimensionless with the saturated bed concentration.

Phenomenological Coefficients. The Peclet number Pe is here regarded as a numerical coefficient to be estimated empirically on the basis of our experimental data. It is worth noting that at large values of the *microscopic* Peclet number

$$\mathrm{Pe}_{\mathrm{micro}} = VA/D_\infty \tag{33}$$

based upon the grain size A, the ratio D_i/D_∞ scales roughly with the first power of $\mathrm{Pe}_{\mathrm{micro}}$ [see, e.g., Yang (24, Eq. 4.15, p. 107); cf. Koch and Brady (27)], whence D_i itself is independent of the value of D_∞. This state of affairs is consistent with the concept of "mechanical dispersion" (27). Thus, since $\mathrm{Pe}_{\mathrm{micro}}$ is large (roughly 170) in our experiments, values of Pe estimated with particles of a given size should apply for all particle sizes.

The effective diffusivity for particle transport within the porous grains is given by an equation of form

$$D_p = D_\infty H/\tau \tag{34}$$

where τ and H denote tortuosity and hydrodynamic hindrance factors, respectively. As a very rough estimate, we take $\tau = 2$ (23, p. 89) and approximate H in terms of the hindrance factor for axial motion of a sphere within a straight circular cylindrical pore, as discussed by Lewellen (28) [see also Deen (29)]; on this basis H is 0.189 for a particle/pore size ratio of 0.5.

The mass transfer coefficient for particle transport from the bulk interstitial fluid to the porous grain surfaces is estimated assuming a microscopic Sherwood number of unity,

$$kA/D_\infty = 1 \tag{35}$$

representing the low-microscopic-Reynolds number limit of standard mass-transfer correlations (24, p. 106) (since the microscopic Reynolds number is of order 0.01 in the small bed).

Solution of the Governing Equations. The solution $c_p(r, z, t)$ of the microscopic porous-phase transport problem (see Eqs. 18, 21, 24, 25, and 30) is expressible analytically in terms of the (as yet unknown) interstitial concentration field $c_i(z, t)$ by the equations (cf. Ref. 30, p. 91)

$$c_p(r, z, t) = c_i(z, t) + \sum_{n=1}^{\infty} A_n(z, t)(\lambda_n r)^{-1} \sin(\lambda_n r) \tag{36}$$

$$A_n(z, t) = e^{-\beta\lambda_n^2 t}[A_n(z, 0) + K_n c_i(z, 0)] - K_n c_i(z, t) + K_n \beta\lambda_n^2 \int_0^t e^{\beta\lambda_n^2(t'-t)} c_i(z, t')\, dt' \tag{37}$$

Here λ_n denotes the nth solution of the transcendental equation

$$\tan(\lambda_n) = \lambda_n/(1 - \kappa) \tag{38}$$

and $A_n(z, 0)$ and K_n respectively denote the nth Fourier coefficients of $c_p(r, z, 0) - c_i(z, 0)$ and 1 with respect to the orthogonal sequence of functions $\{(\lambda_n r)^{-1} \sin(\lambda_n r)\}$, the latter given by

$$K_n = 2\kappa\lambda_n \sin(\lambda_n)[\lambda_n^2 + (\kappa - 1)\sin^2 \lambda_n]^{-1} \tag{39}$$

Thus, the permeation rate $q(z, t)$ is given directly in terms of $c_i(t, z)$ by

$$q(z, t) = -\frac{3(1 - \epsilon_{macro})}{\epsilon_{macro}} \epsilon_{micro} \Phi\beta\kappa \sum_{n=1}^{\infty} A_n(z, t)\lambda_n^{-1} \sin(\lambda_n) \tag{40}$$

The solution of the resulting macroscopic transport problem (see Eqs. 17, 21–23, and 29) is approximated using the method of finite differences with simple Euler time stepping, as is detailed elsewhere (18). Numerical calculations, which use the final condition for each flow (or no-flow) step as the initial condition for the subsequent no-flow (or flow) step, utilize rounded parameter values based on the experimental conditions as listed in Table 1.

Reconciliation of Model with Experiments. The Peclet number Pe for the small bed is determined by matching the preceding model with the measured decaying oscillations in the particle concentration during the approach to partitioning equilibrium (cf. Fig. 7). As is shown by Figs. 12 and 13, the data for 1000 and 520 Å particles are roughly consistent with the numerical value Pe ≅ 5. Figure 12 pertains to 1000 Å particles, modeled assuming impermeable grains, and Fig. 13 corresponds to 520 Å particles, modeled assuming permeable grains with $H/\tau = 0.1$. Figure 14 shows the

TABLE 1
Rounded Parameter Values Used in Numerical Calculations with the Convection-Dispersion-Permeation Model

Φ (for 520 Å particles)	0.19
t_{flow}	0.9
$t_{no\ flow}$	4.0
β (in flow conditions)	4.4 H/τ
κ	7.6/(H/τ)

effect of grain permeability and hindrance upon the predicted transient behavior.

As a check on the value of Pe, Fig. 15 compares predicted eluant concentrations during washing of 1000 Å particles from the small bed, assuming Pe = 5 and impermeable grains, with a corresponding set of wash

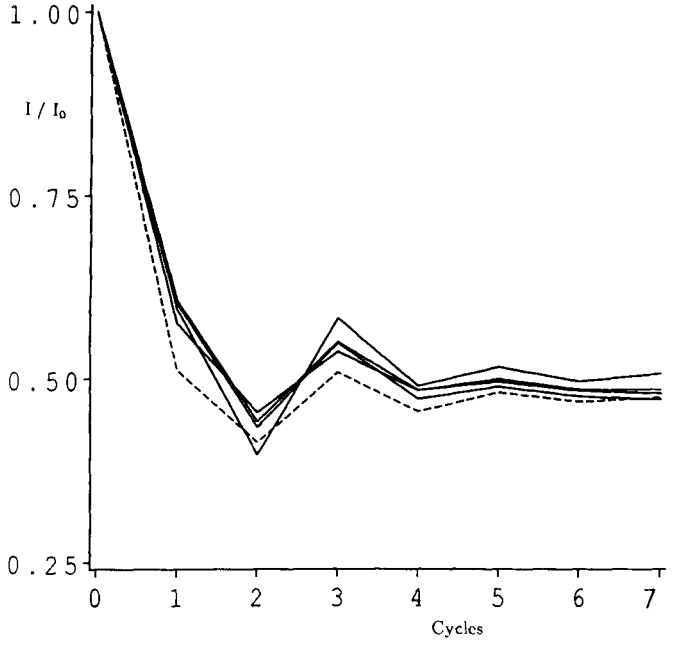

FIG. 12 Experimental data for 1000 Å particles (solid lines) and model prediction (dashed line) with Pe = 5. I/I_0 as a function of the number of cycles.

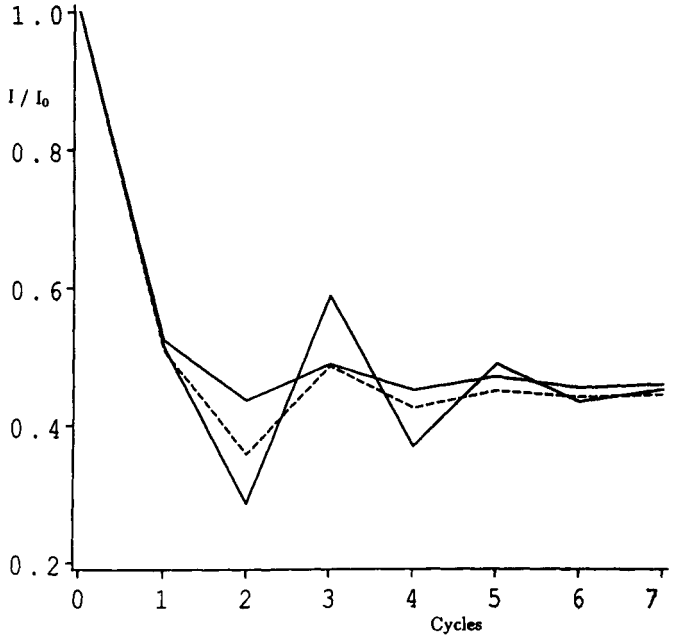

FIG. 13 Two sets of experimental data (solid lines) for 520 Å particles and model prediction (dashed line) based on parameter values listed in Table 1. I/I_0 as a function of the number of cycles.

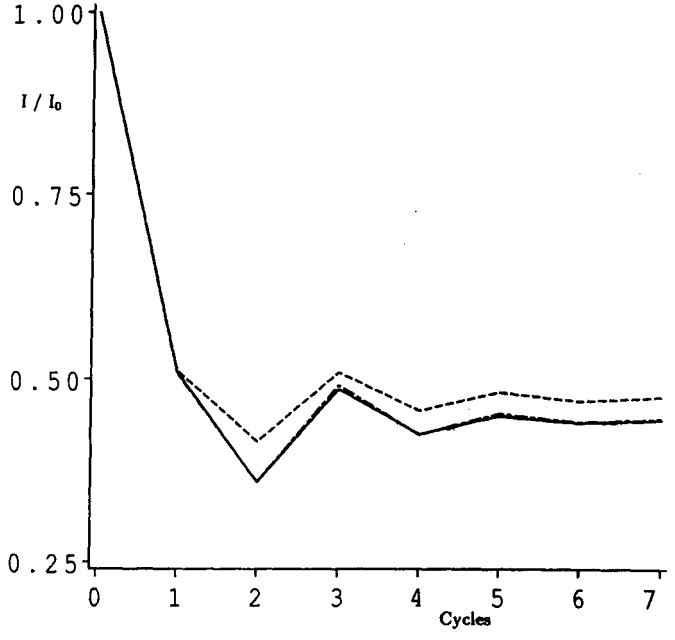

FIG. 14 Model predictions for 520 Å particles with $H/\tau \equiv 0$ (dashed curve), $H/\tau = 0.1$ (solid curve), and $H/\tau = 1.0$ (dot-dashed curve).

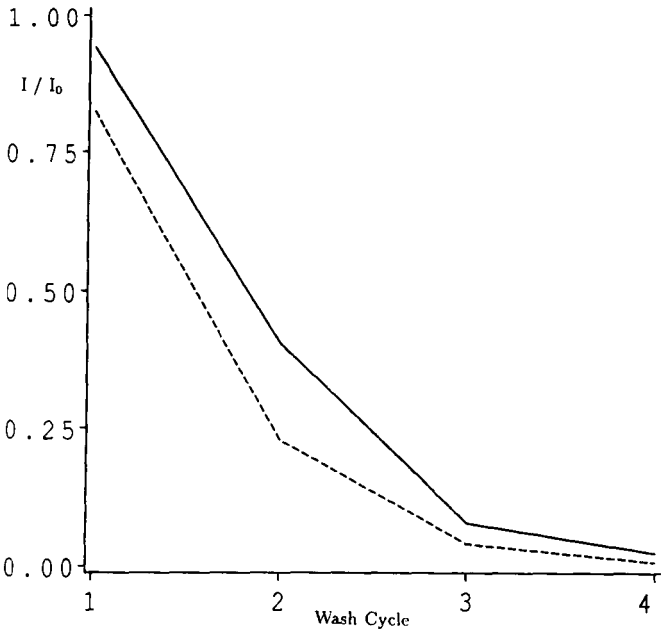

FIG. 15 Predicted (dashed line) eluent concentrations during washing of 1000 Å particles from the bed (Pe = 5.0) compared with experimental data (solid line).

data (selected on the basis of good agreement of the saturated bed concentration with the mean measured partition coefficient K). The rough agreement indicates that the estimated value Pe $\cong$ 5 is of the proper order of magnitude. [This value is evidently much smaller than the theory of Koch and Brady (27) would suggest based on a microscopic Peclet number of roughly 170, although it is worth noting that their theory is strictly applicable only to dilute packed beds.]

5. DISCUSSION

The preceding work has established the operating characteristics of countercurrent fractional extraction, based on contact with a porous phase, as a technique for macromolecular or particulate separations. Size and shape exclusion was considered here as the basis of selectivity because of the simplicity of the underlying microscopic physics (simple steric exclusion). Selectivity by this mechanism is low (i.e., differences in parti-

tion coefficient between different particles are small). This difficulty is exacerbated by the fact that part of the porosity of the porous phase derives from the nonselective interstitial voids, although selectivity is maximized through the use of a material with an essentially uniform pore size distribution (see Ref. 17). It is important to emphasize that the technique advocated here is applicable to any partitioning mechanism, and would require fewer stages for cases of affinity-based, ion-exchange, or other separations for which selectivity is generally much higher. The key observation to make is that stagewise countercurrent contact does not suffer the scale-up limitations that limit chromatographic systems. The development of large-scale multicomponent protein and particle separations by fractional extraction represents a promising and rich area for technological advancement, toward which this work represents a step, and which has already seen considerable investigation [e.g., Chang et al. (7)].

A number of specific conclusions can be derived from the present investigation. First, it seems to be possible to achieve complete equilibration between substantial volumes of liquid and porous phases within a few contacting cycle times. Second, reflux and concentration of an intermediate stream offer improvements in selectivity, although only by a factor of 2 or so and at the expense of practical penalties (such as a much larger stage size needed in the case of reflux). It may therefore be best to increase selectivity simply by increasing the number of stages. Third, dispersion in the bed is intermediate between the extremes of plug flow and perfect mixing, and can be described to reasonable accuracy by a one-dimensional, time-dependent convection-dispersion model. The Peclet number characterizing our experiments with the small bed seems to be approximately 5.

ACKNOWLEDGMENTS

Support of all phases of the work described herein by the National Science Foundation through a Young Investigator (NYI) Award to J.M.N., and by the Procter & Gamble company through a grant under its NYI Support Program, is gratefully acknowledged. The authors express their appreciation to CPG, Inc. for a donation of controlled-pore glass, and for a further supply of this material under very generous terms. Useful discussions with Bang's Laboratories, Inc. concerning handling of particles and with Dr. Durgesh Vaidya concerning the finite difference scheme are gratefully acknowledged. Thanks are also due to Mr. Frank Hicklin for fabrication of the experimental apparatus.

SYMBOLS

a	characteristic solute size
A	radius of grain
$A_n(z, t)$	Fourier coefficient
C_i, c_i	particle concentration in interstitial voids
C_p, c_p	particle concentration in pores of porous grains
C_{bulk}	particle concentration of initial suspension
D_i	dispersion coefficient
D_p	effective diffusivity of particles within the grains
D_∞	particle diffusivity in bulk fluid
F	volumetric flow rate of feed
H	hydrodynamic hindrance factor
I	turbidity in nephelometric turbidity units (n.t.u.)
k	mass-transfer coefficient
K	partition coefficient
K_n	Fourier coefficient
L	length of packed bed
M	total number of stages to the left of the feed stage
N	total number of stages to the right of the feed stage
P, $\overline{P}$	volumetric flow rate of wetted porous phase
Pe	Peclet number
q	rate of mass transfer
Q_S	flow rate of solvent
R, r	microscopic radial coordinate
R_p	micropore radius
S, $\overline{S}$	volumetric flow rate of solvent phase
$\mathcal{S}$	selectivity
T, t	time
T_{flow}	time of flow through bed
$T_{no\ flow}$	time of no flow through bed
V	mean fluid flow velocity
V_I	interstitial bed volume
V_p	porous phase volume
V_0	initial volume of suspension
x, $\overline{x}$	solute concentration in solvent phase
y, $\overline{y}$	solute concentration in porous phase
Z, z	axial position in packed bed

Greek Symbols

β	dimensionless group defined by Eq. (20)

ϵ	overall porosity
ϵ_{macro}	macroscopic porosity
ϵ_{micro}	microscopic porosity
κ	dimensionless mass transfer coefficient defined by Eq. (26)
λ_n	eigenvalues defined by Eq. (38)
Φ	single-pore partition coefficient
τ	tortuosity

REFERENCES

1. H. G. Barth and B. E. Boyes, "Size Exclusion Chromatography," *Anal. Chem.*, *62*, 381R–394R (1990).
2. P. L. Dubin, *Aqueous Size-Exclusion Chromatography* (Journal of Chromatography Library, Vol. 40), Elsevier, New York, NY, 1988.
3. A. C. Gadkari, M. Zsuga, and J. P. Kennedy, "Preparative GPC in Fundamental Polymer Synthesis," *Polym. Bull.*, *18*, 317–322 (1987).
4. W. G. Sisson, J. M. Begovich, C. H. Byers, and C. D. Scott, "Continuous Chromatography," *Chemtech.*, *18*, 498–502 (1988).
5. L. O. Lindquist and K. W. Williams, "Aspects of Whey Processing by Gel Filtration," *Dairy Ind. Int.*, *38*, 459–464 (1973).
6. H. Friedli and P. Kistler, "Removal of Ethanol and Salt from Albumin by Gel Filtration," in *Methods of Plasma Protein Fractionation* (J. M. Curling, Ed.), Academic Press, New York, NY, 1980, pp. 203–210.
7. Y. K. Chang, G. E. McCreath, N. M. Draeger, and H. A. Chase, "Novel Technologies for Direct Extraction of Proteins," *Trans. Inst. Chem. Eng.*, *71A*, 299–303 (1993).
8. J.-X. Huang and G. Guiochon, "Applications of Preparative High-Performance Liquid Chromatography to the Separation and Purification of Peptides and Proteins," *J. Chromatogr.*, *492*, 431–469 (1989).
9. J.-C. Janson and P. Hedman, "Large-Scale Chromatography of Proteins," in *Chromatography* (Advances in Biochemical Engineering, Vol. 25) (A. Fiechter, Ed.), Springer-Verlag, New York, NY, 1982, pp. 43–99.
10. R. E. Treybal, *Liquid Extraction*, McGraw-Hill, New York, NY, 1951.
11. D. M. Ruthven, *Principles of Adsorption and Adsorption Processes*, Wiley, New York, NY, 1984, Chap. 12.
12. B. B. Fish, R. W. Carr, and R. Aris, "The Continuous Countercurrent Moving-Bed Separator," *AIChE J.*, *35*, 737–745 (1989).
13. B. B. Fish, R. W. Carr, and R. Aris, "Optimization of the Countercurrent Moving-Bed Chromatographic Separator," *Ibid.*, *39*, 1621–1627 (1993).
14. W. L. McCabe, J. C. Smith, and P. Harriott, *Unit Operations of Chemical Engineering*, 5th ed., McGraw-Hill, New York, NY, 1993.
15. J. R. Pappenheimer, E. M. Renkin, and L. M. Borrero, "Filtration, Diffusion and Molecular Sieving through Peripheral Capillary Membranes: A Contribution to the Pore Theory of Capillary Permeability," *Am. J. Physiol.*, *167*, 13–46 (1951).
16. E. M. Renkin, "Filtration, Diffusion, and Molecular Sieving through Porous Cellulose Membranes," *J. Gen. Physiol.*, *38*, 225 (1954).
17. J. M. Nitsche and K. W. Limbach, "Partition Coefficients for Distribution of Rigid Non-axisymmetric Solutes between Bulk Solution and Porous Phases: Toward Shape-Selective Separations with Controlled-Pore Materials," *Ind. Eng. Chem. Res.*, *33*, 1391–1396 (1994).

18. P. Roy, "On the Separation of Spherical and Nonspherical Particles by Partitioning and Flow Phenomena," Doctoral Dissertation, State University of New York at Buffalo, 1996.
19. J. C. Giddings, E. Kucera, C. P. Russell, and M. N. Myers, "Statistical Theory for the Equilibrium Distribution of Rigid Molecules in Inert Porous Networks. Exclusion Chromatography," *J. Phys. Chem.*, *72*, 4397–4408 (1968).
20. M. T. Bishop, K. H. Langley, and F. E. Karasz, "Dynamic Light-Scattering Studies of Polymer Diffusion in Porous Materials: Linear Polystyrene in Porous Glass," *Macromolecules*, *22*, 1220–1231 (1989).
21. D. R. Bauer, "Hydrodynamic Properties of Dilute and Concentrated Polymer Latexes: A Study by Quasielastic Light Scattering," in *Polymer Colloids II* (R. M. Fitch, Ed.), Plenum Press, New York, NY, 1980, pp. 51–69.
22. R. H. Perry, D. W. Green, and J. O. Maloney (Eds.), *Perry's Chemical Engineers' Handbook*, 6th ed., McGraw-Hill, New York, NY, 1984.
23. W. W. Yau, J. J. Kirkland, and D. D. Bly, *Modern Size-Exclusion Liquid Chromatography: Practice of Gel Permeation and Gel Filtration Chromatography*, Wiley, New York, NY, 1979.
24. R. T. Yang, *Gas Separation by Adsorption Processes*, Butterworths, Boston, MA, 1987.
25. R. A. Novy, H. T. Davis, and L. E. Scriven, "Upstream and Downstream Boundary Conditions for Continuous-Flow Systems," *Chem. Eng. Sci.*, *45*, 1515–1524 (1990).
26. H. Brenner, "The Diffusion Model of Longitudinal Mixing in Beds of Finite Length. Numerical Values," *Ibid.*, *17*, 229–243 (1962).
27. D. L. Koch and J. F. Brady, "Dispersion in Fixed Beds," *J. Fluid Mech.*, *154*, 399–427 (1985).
28. P. C. Lewellen, "Hydrodynamic Analysis of Microporous Mass Transport," Doctoral Dissertation, University of Wisconsin-Madison, 1982.
29. W. M. Deen, "Hindered Transport of Large Molecules in Liquid-Filled Pores," *AIChE J.*, *33*, 1409–1425 (1987).
30. J. Crank, *The Mathematics of Diffusion*, 2nd ed., Oxford University Press, Oxford, 1975.

Received by editor July 12, 1996
Revision received February 21, 1997